MECHANICAL AND TRIBOLOGICAL PROPERTIES OF INJECTION MOLDED ZIRCONIA-ALUMINA FOR ORTHOPEDIC IMPLANTS

Anna Rita Terrizzi[1], Maurizio Fersini [2], Vincenzo Contaldi[2], Sanosh Kunjalukkal Padmanabhan[1], Mari-Ann Einarsrud[3], Antonio Alessandro Licciulli[1]

[1] Department of Innovation Engineering, University of Salento, 73100 Lecce, Italy

[2] Salentec s.r.l., 73100 Lecce, Italy

[3] Department of Materials Science and Engineering, NTNU Norwegian University of Science and Technology, 7491 Trondheim, Norway

*   Correspondence: e-mail: annarita.terrizzi@unisalento.it; Tel.: +39 3889959130

Abstract

Ceramics have gained great attention for hip and knee arthroplasty surgical procedures due to their ability to guarantee long-life performance in patients and considered an alternative to existing metal systems.

In the present study, zirconia toughened alumina (ZTA) for orthopaedic implants has been developed by Ceramic Injection Molding (CIM) process and characterized. Microstructural, mechanical and tribological studies have been carried out to establish whether the material is suitable for the purpose. The new CIM ZTA material obtained density up to 99.4%, toughness 6.1 MPa·m$^{1/2}$, hardness 20 GPa, Young's modulus 320 GPa, and low coefficient of friction ranging between 0.08 and 0.13 under lubricated conditions, and between 0.11 and 0.34 in dry condition. To simulate the performance of the ZTA *in vivo*, i.e., the influence of material degradation on the ageing properties, accelerated hydrothermal aging was performed in vitro and good mechanical and tribological properties were confirmed for the developed ZTA.

Keywords: orthopedic implants; zirconia toughened alumina; ceramic injection molding; mechanical properties; tribological properties.

1 Introduction

Total Hip Arthroplasty (THA) and Total Knee Arthroplasty (TKA) are the most successful surgical procedures used to restore the proper functioning of the joints and to guarantee patient mobility, especially where severe forms of arthrosis occur. The global forecast for the use of implants for both females and males is expected to increase in the United States by 75%, 129%, and 284% for primary THA, and by 110%, 182%, and 401% for primary TKA, in 2025, 2030, and 2040, [1], [2]. A discrete-event prediction model has been developed to represent TKA use over 20 years (2012-2031) in the Spanish national health system and the increase of the revision intervention has been predicted [3]. From the first cases, important advances in implant materials and design have improved the longevity of these devices.

The first Metal-on-metal (MoM) prosthesis with large-diameter femoral head date back to 1955-1965 [4], and the first total hip replacement dates 1960, consisted of a metal femoral head and an acetabular cemented polyethylene (PE) [5]. The main problem of the metal-PE system (MoP) is the limited life time of the device of about 10-15 years, due to the formation and loosening of wear particles in osteolysis [6].

Studies are required to increase the life expectancy of the implant, in order to obtain long-lasting prostheses that can also be implanted in young and active patients [7]. The search for alternative materials that offer high mechanical resistance, optimal tribological properties, long-term biocompatibility, and minimize issues such as biological reactions against wear particles, is a relevant challenge [8], [9].

The use of advanced ceramics for biomedical devices dates back to the 1970s when the French surgeon Pierre Boutin introduced the alumina femoral head in hip implants in a ceramic-on-ceramic (CoC) coupling [10], [11] as an alternative to metal systems.

Alumina ceramics offered low friction in all ceramic bearings, biological safety, stiffness, long term stability, and better wettability compared to metal alloys such as CoCrMo [12], contributing to a reduced rate of aseptic loosening and osteolysis, which are the major threats in metal couplings [13], [14]. Wear of alumina implant was only a few microns over a 15-year period of use, which is 2000 times less than a MoP and 100 times less than a MoM prosthesis [15]. Despite the improved biocompatibility and tribology, alumina has low strength [16], and a high fracture rate due to crack growth [17], [18].

In the 1980s, zirconia femoral head (ZrO_2) became an alternative to alumina, due to good chemical stability, higher flexural strength and fracture toughness [17]. Unfortunately, it was later discovered that zirconia was hydrothermally weakened and long-term stability decreased, resulting in an increased risk of fracture and degradation of wear properties [19]–[21].

To combine the hardness of alumina with the toughness of zirconia and to overcome the aging sensitivity of zirconia, zirconia-toughened alumina (ZTA) composites were developed in the 1990s for hip replacement bearings [22].

ZTA composites exhibit higher fracture toughness and fatigue strength compared to alumina [23]–[26]. Combined with low wear rate and excellent long term biocompatibility, ZTA composites are very interesting candidates to be used in arthroplasty applications [27]–[29] and as joint couplings in ceramic on polyethylene (CoP) THA [30].

In this work, ZTA for TKA was developed using Ceramic Injection Molding (CIM) following the guidelines of ISO standard for materials for medical devices, i.e., an alumina content of 60-90 wt%, zirconia content in the range 10-30 wt% and other additives $\leq$ 10 wt% [31]. CIM, an interesting process for the manufacturing of ceramics allowing mass production of complex components, was used for the green body shaping [32].

The aim of the study was to characterize CIM derived ZTA and evaluate mechanical and tribological performance and establish whether it is suitable for orthopedic devices. To simulate the performance of the ZTA materials *in vivo* and to investigate degradation due to aging, the stability of the materials was evaluated through accelerated hydrothermal aging at elevated temperature. The influence of the CIM shaping process for the improvement of properties of the ceramics is discussed.

2 Materials and methods

2.1 Material preparation

Zirconia Toughened Alumina (ZTA) with Al_2O_3 (83 vol%) and ZrO_2 (17 vol%) test specimens and components have been prototyped by ceramic injection molding in Salentec srl. Alumina (Alteo, P172LSB, P172HPB; mean particle size ~400 nm) and 3 mol% yttria-stabilized zirconia powders (Zirox - DTSE3; mean particle size 500 - 1500 nm) were spray-dried and compounded with a proprietary mix of thermoplastic binders based on low-density polyethylene (LDPE) and water-soluble waxes, to prepare a homogeneous feedstock. The feedstock was pre-heated and injected at 1000 bar into a mold, to obtain complex shape components and test specimens.

Water dewaxing and organics burnout were performed after molding for removing water-soluble waxes and high temperature melting binders, respectively. The obtained bodies were sintered in air at 1475°C in a laboratory furnace for 75 min and mirror-polished for 24 h in a disc finishing machines (Otec) using 40 µm size diamond powder. Density of sintered specimens was determined using Archimedes' method.

Selected samples were subjected to accelerated aging in an autoclave by applying pressurized water vapor at 0.2 MPa and 134 ± 2°C, for 10 h according to ISO 6474-2:2019 (E) for ceramic materials suitable for medical surgery. The number and dimensions of the samples, the characterization methods used to evaluate the microstructural, phase composition and mechanical properties are shown in *Table 1*.

Characterization technique	*Number of samples*	*Dimension of samples [mm^3]*	*Evaluated material properties*
Scanning electron microscopy (SEM)	1 non-aged	40 x 4 x 3.15	Microstructure
X-ray diffraction	1 non-aged 1 aged	10 x 4 x 3.15	Fraction of zirconia monoclinic phase
Raman spectroscopy	1 non-aged 1 aged	10 x 4 x 3.15	Fraction of zirconia monoclinic phase
Three-point bending test (3PB-test)	10 non-aged 10 aged	40 x 4 x 3.15	Flexural strength Weibull modulus Young's modulus
Three-point bending test using strain gauge	2 non-aged	100 x 10 x 3.50	Young's modulus
Vickers indentation	2 non-aged	40 x 4 x 3.15	Hardness
Single-edged V-notch beam test (SEVNB test)	5 non-aged 5 aged	40 x 4 x 3.15	Fracture toughness
Tribological test (pin on disk)	6 non-aged 6 aged	60 x 10 x 3.50	Friction coefficient Wear rate Roughness

Table 1. Overview of characterization methods used and evaluated properties.

2.2 Scanning electron microscopy (SEM)

Scanning electron microscopy (Carl Zeiss Microscopy Ltd. System model ΣIGMA™VP; accelerating voltage of 10 kV, working distances of 11-12 mm) was used to evaluate morphology and estimate grain size of sintered ZTA. The sintered and polished samples were thermally etched in air at 1450 °C using a heating rate of 4.5 °C/min previous to SEM analysis. The grain size distribution was evaluated using the micrographs and the image processing tool ImageJ and the average grain size of alumina and zirconia grains was estimated by the interception method.

2.3 Evaluation of monoclinic zirconia content

Two different methods were used to evaluate the conversion of the zirconia tetragonal phase to monoclinic after accelerated aging. In the first method, X-ray diffraction (XRD) patterns were recorded using a diffractometer (BRUKER D8 Advance, Da Vinci design) with Cu-Kα radiation, a voltage of 40 kV, a current emission of 20 mA, in a range (θ-2θ) between 20 and 90° with a step size of 0.02° and acquisition time of 2 sec per step. Rietveld refinements were carried out on the raw data using the Bruker TOPAS software (version 64V6) [33].

In the second method, Raman spectra (Witec alpha 300r) were recorded using a laser excitation source of 532 nm and collecting 5 spectra for each ZTA sample.

2.4 Three-point bending tests

Flexural strength was measured by three-point bending tests (3PB-test). Weibull modulus and Young's modulus of the ZTA were evaluated according to ASTM C1161, UNI EN 843-2:2006, using a servo-hydraulic mechanical test machine (MTS Minibionix 858, 10 kN load cell) at a displacement rate of 0.5 mm/min (*Figure 1a*). Young's modulus was measured using a one-way linear strain gauge (HBM 1-CLY41-3/120ZE series) fixed on the sample and connected to an acquisition unit (HBM QuantumX MX1615B) (*Figure 1b*). Scanning electron microscopy (HITACHI S-4000; accelerating voltage of 10 kV, working distances of 6 -10 mm), was used to observe the fracture surface of the tested samples to identify the fracture mechanism. To obtain good resolution micrographs, surfaces were sputter-coated with gold (EDWARDS Sputter Coater S150B, 9 Volts, 5 mA, ~ 0.15 atm).
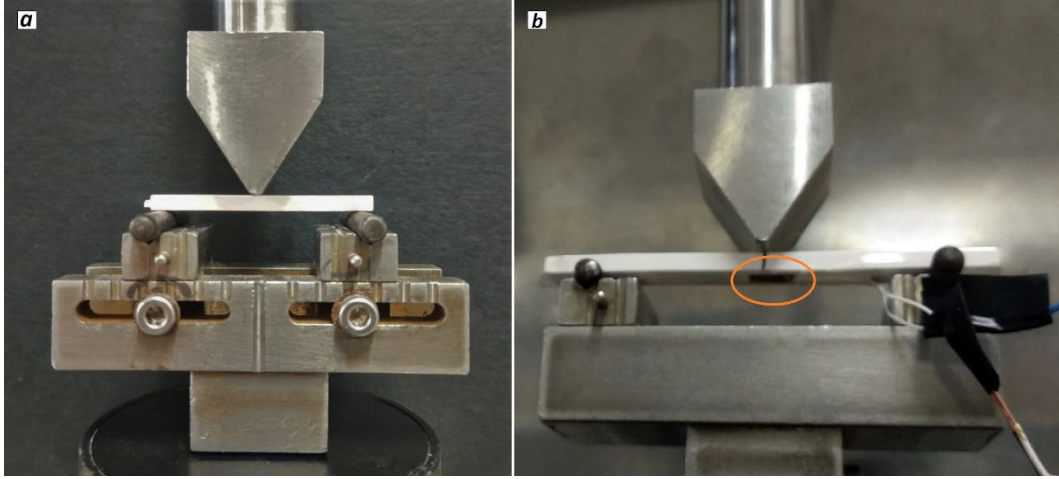
Figure 1. Setup for 3PB-test (a) and 3PB-test with strain gauge (b).

2.5 Vickers indentation tests

Vickers hardness tests were performed at room temperature using a hardness tester (WIKI 200 JS, AFFRI), with natural diamond machined at 136° following ISO 14705:2016 (E). The force was applied electronically through load cells and controlled in Closed Loop (frequency of 1 kHz) and automatically generating imprints.

The tests were performed with a load of 9.81 N, according to ISO 6474-2:2019 and ASTM C1327-99, for a duration of 15 sec. Vickers hardness (HV1), expressed in GPa, was calculated by equation (1):

$$HV1 = 0.0018544 \left(\frac{P}{d^2}\right) \tag{1}$$

where P is the applied load (N), d is the average length of the two diagonals of the resulting indent (mm). Indented diagonals were measured using a scanning electron microscope (Carl Zeiss Microscopy Ltd. System model ΣIGMA™VP). The average value was calculated from five different measurements on each sample.

2.6 Single-edge V-notch beam tests

The fracture toughness ($K_{Ic,SEVNB}$) was evaluated using the Single-edge V-notch beam method (SEVNB) according to the standards UNI EN ISO 23146:2016 [34]. Bars with a 0.5 mm deep notch made by computer numerical control (CNC) milling (0.25 mm thick blade) followed by making a V-shaped notch by hand (from 0.1 to 0.2 mm thick blade; 1 μ diamond paste). The notch depth was measured by a digital optical microscope (PCE-MM200).

Three-point tests were performed by a servo-hydraulic uniaxial press (MTS Minibionix 858, 10 kN load cell, traverse speed 0.5 mm/min, 40 mm span). Fracture toughness was calculated by equation (2):

$$K_{Ic,SEVNB} = \frac{F}{B\sqrt{W}} \cdot \frac{S_1}{W} \cdot \frac{3\sqrt{\alpha}}{2(1-\alpha)^{1.5}} Y \tag{2}$$

where F is the fracture load (MN), B is the test-piece width (m), W is the test-piece depth (m), S_1 is the support span (m), α = a/W is the relative V-notch depth, a is the average V-notch depth (m) measured after the test, $Y = 1.9472 - 5.0247\alpha + 11.8954\alpha^2 - 18.0635\alpha^3 + 14.5986\alpha^4 - 4.6896\alpha^5$ is the stress intensity shape factor (a dimensionless term determined by the crack configuration and loading geometry).

2.7 Friction and wear investigation

The tribological tests were performed using a tribometer (NANOVEA T500) in "pin on disk" configuration following standard ISO 6474-2:2019 [31]. Load condition, time, and velocity were either controlled or monitored during the test [23], [35], [36].

ZTA ceramic cylindrical pins (diameter 4 mm) with a rounded tip and six ZTA samples were used for the test. Three unaged and three samples were subjected to accelerated aging by hydrothermal treatment were tested.

Test configuration consisted of the pin perpendicular to the sample moving on a rotating platform. The rotation under the pin at a controlled load produced a circular wear track on the surface with a set radius of 3.00 mm.

The test duration was 120 min at a speed of 100 mm/s at three different loads (10, 20 and 40 N) in dry (*Figure 2a*) and lubricated conditions (*Figure 2b*) using bovine calf serum (BCS, Sigma-Aldrich, 12133C, total protein range 5.8 – 7.1 g/dL). Friction coefficients were acquired by a frequency sampling of 0.2 Hz. At the end of the test, the sample was removed from the tribometer, dried with airflow, cleaned using acetone and fired at 550 °C for 30 min to remove organic substances absorbed during the test.
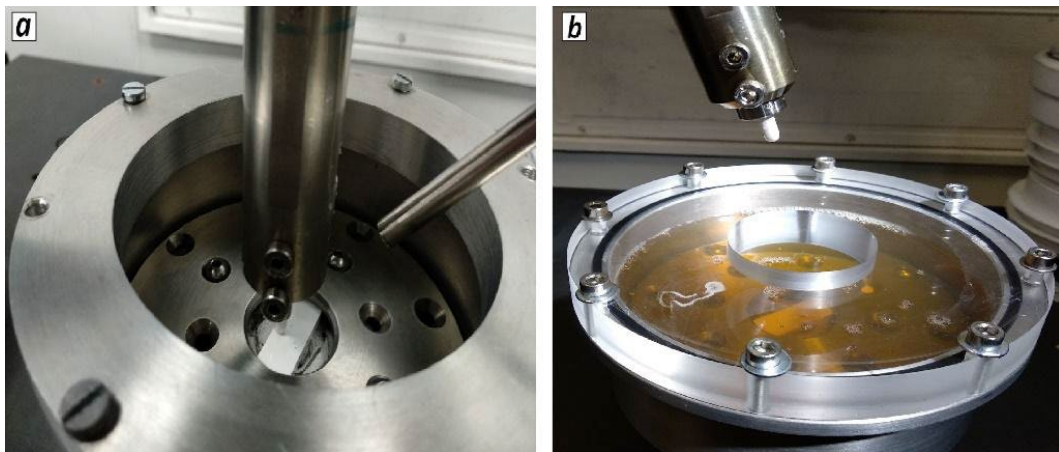
*Figure 2. The test set up in dry (a) and bovine calf serum (BCS) configuration (b).*

Wear track images were obtained by scanning electron microscopy (Carl Zeiss Microscopy Ltd. System model ΣIGMA™VP; accelerating voltage of 15 kV, working distances of 9 -14 mm), to examine the surface after the tribological test.

Ten radial profiles on each wear track (one every 36 degrees) were acquired by a profiler (Bruker, DektakXT) to investigate the surface roughness (*Ra*), the maximum depth (*h*) and the width. Using this data, a model was created to calculate the wear rate after testing.

3 Results

3.1 Microstructure, density and grain size

SEM image of the fracture surface of ZTA shows a macrostructure with the presence of some voids (*Figure 3a*); these were probably caused by the incomplete filling of the mold during injectionprocess. Although some pores are present, the sintered samples have a density of 99.4% of the theoretical density. SEM micrograph (*Figure 3b*) shows a fine and homogeneous microstructure and well-dispersed alumina and zirconia grains in the ZTA identified by dark and white color, respectively. An alternation of larger alumina grains (grey) with sharp and defined contours, surrounded by smaller zirconia grains (white) homogeneously distributed are shown. Mean grain size is 1.15 ± 0.04 µm and 0.60 ± 0.01 µm for alumina and zirconia, respectively (*Figure 3c, Figure 3d*).
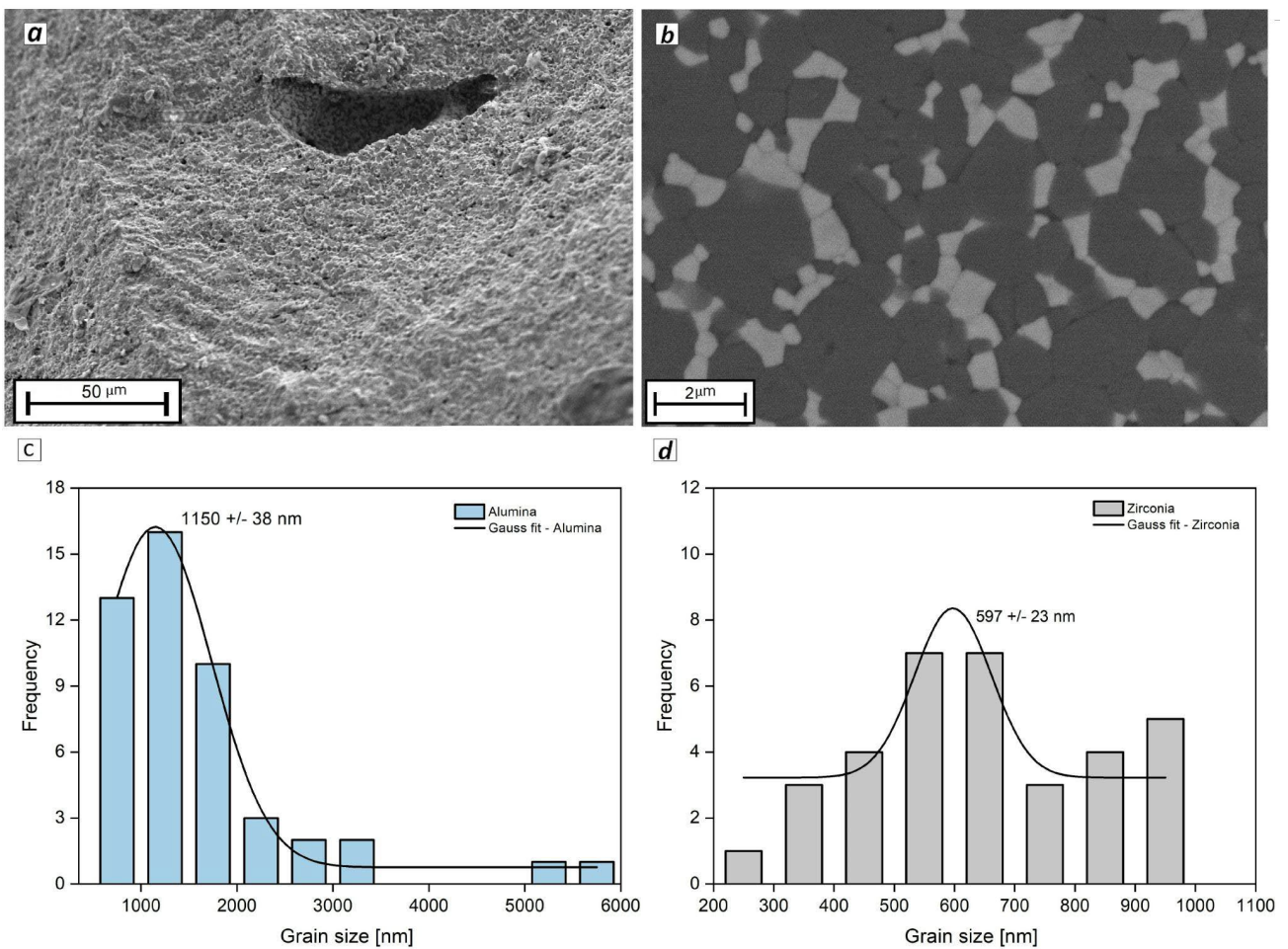
Figure 3. A pore in the fracture surface (a) and backscattered micrograph of microstructure (b). The grain size of alumina (c) and zirconia (d) in ZTA.

3.2 Monoclinic zirconia content

The amount of monoclinic and tetragonal zirconia phases was estimated by XRD and Raman spectroscopy.

The X-ray diffractograms are shown in *Figure 4a* and the monoclinic zirconia content, X_m, was calculated with the Toraya and Yoshimura equation (3):

$$X_m = \frac{I_m(\bar{1}11) + I_m(111)}{I_m(\bar{1}11) + I_m(111) + I_t(101)} \tag{3}$$

where $I_m(\bar{1}11)$ is the monoclinic peak intensity ($2\theta \approx 28.2°$), $I_m(111)$ is the monoclinic peak intensity ($2\theta \approx 31.3°$) and $I_t(101)$ tetragonal peak intensity ($2\theta \approx 30.2°$) [37], [38].

The monoclinic phase fraction was also quantified from Raman spectra using the Katagiri equation (4) where I_m^{178}, I_m^{189}, I_t^{145} are, respectively, the Raman band intensities of the monoclinic bands at 178 and 189 cm^{-1} and peak intensity of the tetragonal band at 145 cm^{-1} [23]:

$$X_{mK} = \frac{(I_m^{178} + I_m^{189})}{4.4 I_t^{145} + I_m^{178} + I_m^{189}} \tag{4}$$

In the Raman spectra (*Figure 4b*), a small increase in the intensity of the bands of monoclinic ZTA (178 and 189 cm^{-1}) and a decrease of the tetragonal phase band (145 cm^{-1}) are evident in the aged ZTA.
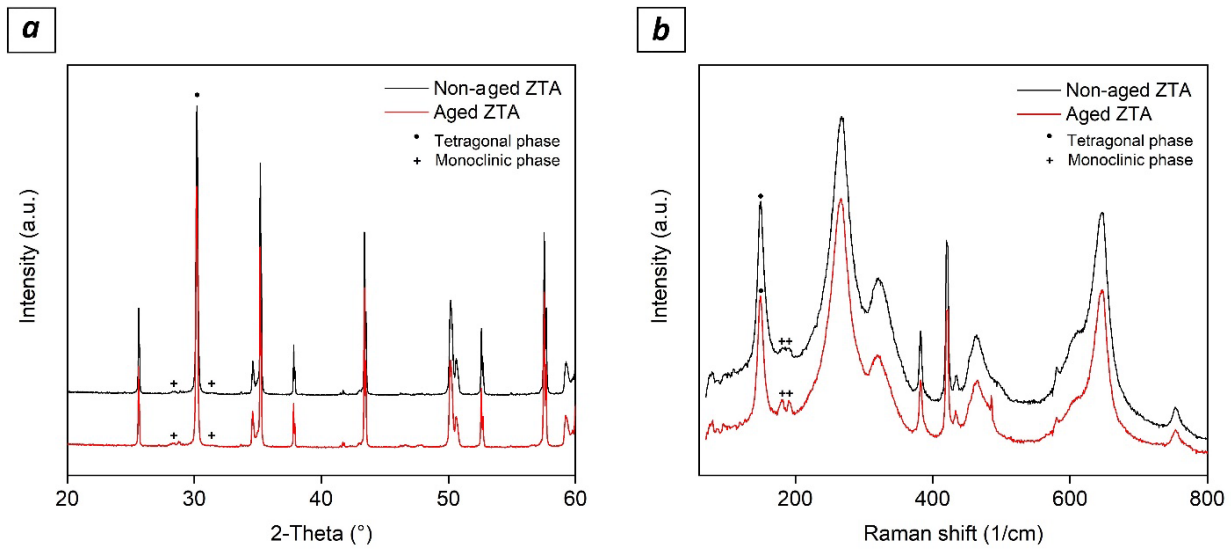
Figure 4. X-ray diffractograms (a) and Raman spectra (b) of non-aged and aged ZTA samples.

The results show a consistent low monoclinic phase content of 3.2 and 3.5 % using XRD, and 3.4 and 4.5% by Raman spectroscopy for non-aged and aged samples respectively (*Table 2*).

Sample	% Monoclinic phase by XRD diffraction	% Monoclinic phase by Raman spectroscopy (Mean content ± standard deviation)
Non-aged ZTA	3.2 ± 0.2	3.4 ± 0.3
Aged ZTA	3.5 ± 0.3	4.5 ± 0.4

Table 2. Monoclinic zirconia content in non-aged and aged ZTA materials.

3.3 Mechanical properties

Weibull modulus, Young's modulus, hardness and fracture toughness measured both before and after aging fulfilled the standard requirements [31]. Flexural strength (~500 MPa) and Young's modulus (320 GPa) are similar for the two types of samples.

Mechanical properties	Non-aged ZTA	Aged ZTA
Flexural strength [MPa]	515 ± 30	500 ± 35
Weibull modulus	>17	8.4
Young's modulus [GPa] (confirmed by test with strain gauge technique)	320	320
Hardness (HV1) [GPa]	20 ± 1	-
Toughness (SEVNB test) [MPa·m$^{1/2}$]	6.1 ± 0.5	5.6 ± 0.2

Table 3. Mechanical properties of ZTA samples not subjected and subjected to accelerated ageing.

Fracture surfaces (after three 3PB-tests) investigated by SEM identified the fracture origin as near-surface or internal pores typical for crystalline ceramics. Griffith's fracture model for brittle materials was considered assuming the pores as the fracture origin. Griffith's equation (5) was used where the fracture strength (σ_f) depends on the defect size c, Young's modulus E and the fracture energy γ:

$$\sigma_f = \sqrt{\frac{2E\gamma}{\pi c}} \tag{5}$$

The comparison between the stress σ_d calculated at the defect location at distance *d* from the applied maximum tensile stress, and the flexural strength estimated by equation (5) at the same distance *d*, is shown in *Table 4*. The difference Δ between the estimated stress and the stress measured during the bending tests is very low. Good correspondence between the stress at the defect and the strength estimated is observed.

Sample	Fracture origin	Defect size (c) [μm]	Distance (d) [μm]	Fracture energy (γ) [J/m^2]	Strength estimated by Griffith equation (σ$_f$) [MPa]	Stress at defect (σ$_d$) [MPa]	Δ [%]
Non-aged 1	Internal pore	68	249	5.5E-05	409	398	3
Non-aged 2	Internal pore	67	235	5.5E-05	412	398	3
Aged 1	Near - surface pore	30	0	4.7E-05	564	541	4
Aged 2	Near - surface pore	50	0	4.7E-05	437	427	2

Table 4. Flexural strength calculated by 3PB-test and fracture strength estimated by Griffith equation.

From the backscattered SEM images of fracture surfaces (*Figure 5a, Figure 5b*), the individual grains of alumina and zirconia can be recognized. A transgranular fracture mode is observed.
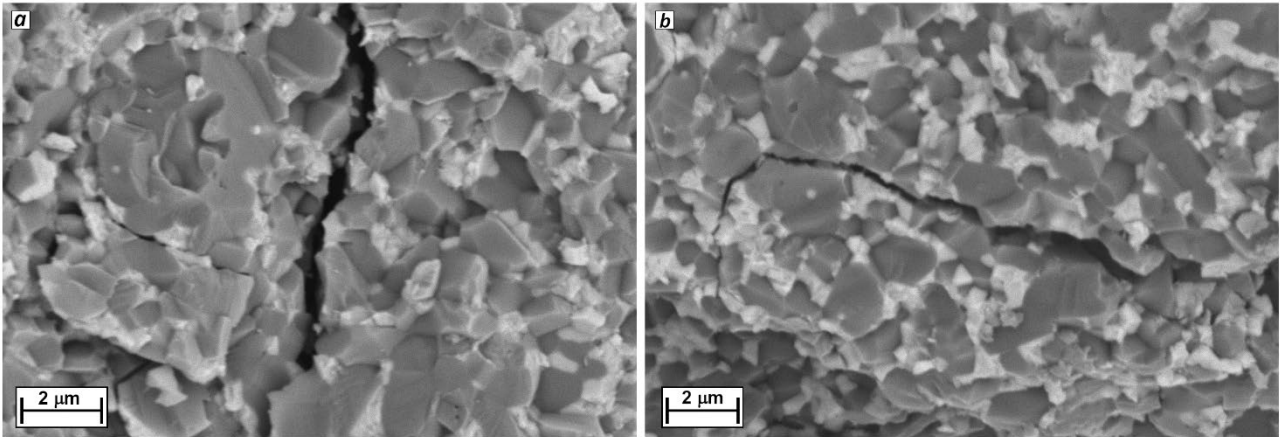

Figure 5. SEM micrographs of fracture surface after three-point bending test. Transgranular fracture mode is evidenced.

3.4 Tribological investigation

Results of tribological investigation are presented in terms of the friction coefficients time dependence and wear rate evaluated by measuring the volume of wear tracks and the roughness of the surfaces.
The following sample and test designations have been adopted:
- DRY_Load: sample not subjected to accelerated aging; dry test; load in N;
- BCS_Load: sample not subjected to accelerated aging; test in bovine serum; load in N.
- A-DRY_Load: accelerated aging sample; dry test; load in N;
- A-BCS_Load: accelerated aging sample; test in bovine serum; load in N.

3.4.1 Friction coefficient

The dynamic friction coefficients recorded during the tribological test in dry and lubricated conditions show a stable trend between 6000 and 38000 revolutions. At the same load, the friction coefficient obtained under dry conditions is significantly higher than that obtained under wet conditions (*Figure 6, Figure 7*).
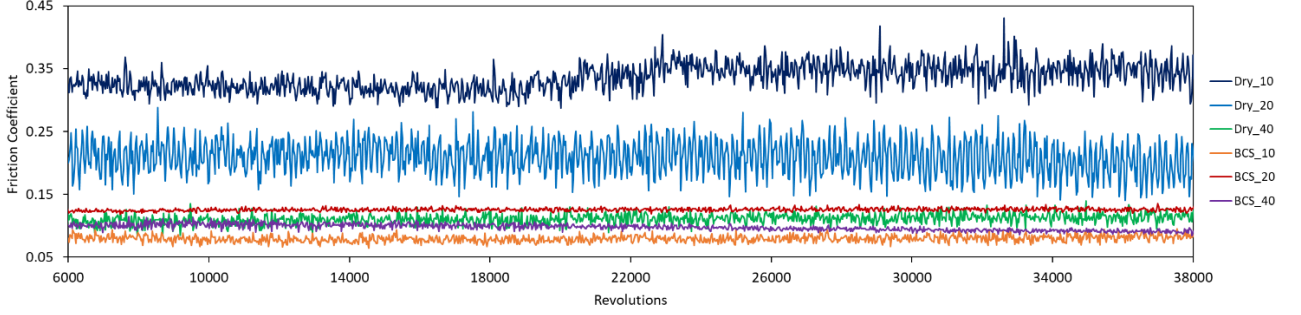

Figure 6. Friction coefficient graph for non-aged ZTA samples. The initial period of 6000 revolutions was removed from the graphs to avoid initial data scattering.
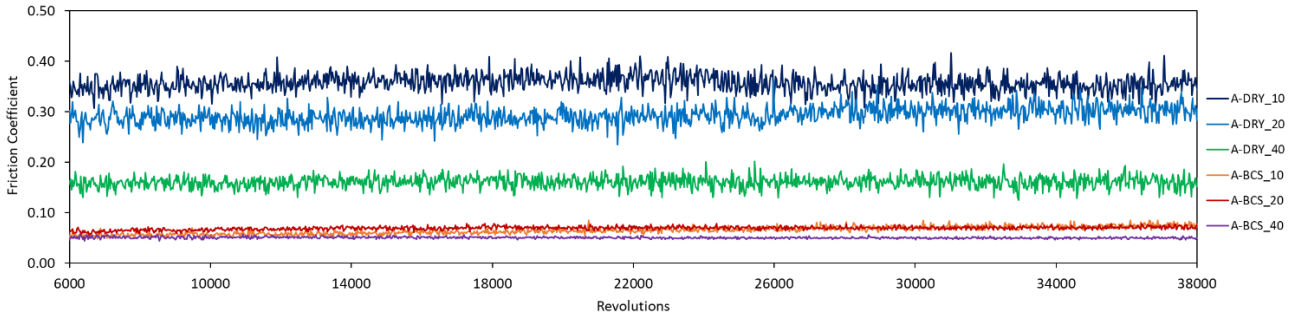

Figure 7. Friction coefficient graph for aged ZTA samples. The initial period of 6000 revolutions was removed from the graphs to avoid initial data scattering.

The mean Hertzian contact pressures, p_m, [39] at the initial instants were calculated by equations (6) and (7):

$$p_m = \frac{F}{\pi a^2} \tag{6}$$

$$a = \left(\frac{3FR}{4E^*}\right)^{1/3} \tag{7}$$

where F is the applied load (N), a is the radius of the contact area (mm), E^* is the contact modulus (MPa), R is the reduced radius of curvature (mm) as given in equations (8) and (9):

$$\frac{1}{E^*} = \frac{(1-v_1^2)}{E_1} + \frac{(1-v_2^2)}{E_2} = \frac{2(1-v^2)}{E} \tag{8}$$

$$\frac{1}{R} = \frac{1}{R_1} + \frac{1}{R_2} \tag{9}$$

where $E_1 = E_2 = E$ is the Young's modulus and $v_1 = v_2 = v$ (0.22) is the Poisson's ratio for pin and sample respectively, and R_1 and R_2 are respectively radius of pin (2 mm) and sample ($= \infty$).

In dry conditions, stable friction coefficients of 0.34, 0.21 and 0.11 were measured for non-aged samples corresponding to Hertzian pressures of 1500, 2000 and 2500 MPa (load 10 N, 20 N, 40 N), while slightly higher values were obtained for aged samples (*Figure 8a*). For lubricated test specimens, the mean friction coefficient (about 0.08) did not show a significant change with varying load (*Figure 8b*).
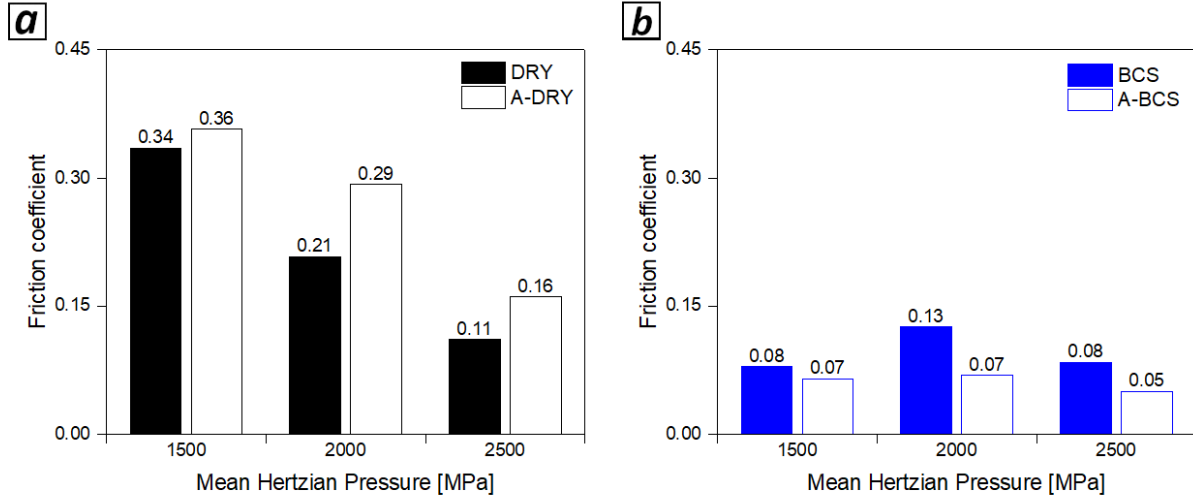

Figure 8. Mean friction coefficient of non-aged and aged ZTA in dry conditions (a) and lubricated conditions (b).

3.4.2 Wear evaluation

The average wear rate (k_w) was calculated as the ratio of the volume loss (V_w) and the total sliding distance (s = 720 m) and the applied force (F) [40], *i.e.*, by equation (10). Since microscopy images show that the track width was nearly constant (*Figure 9a*), a geometrical model was elaborated. The wear volume was calculated by equation (11), i.e. the sum of the ten volumes v_i [mm^3] into which the circumference is divided (*Figure 9b*).

$$k_w = \frac{V_w}{Fs} \qquad (10)$$

$$V_w = \sum_{i=1}^{i=10} v_i = \sum_{i=1}^{i=10} a_{t_i} l_i \qquad (11)$$

where l_i and a_{ti} are, respectively, the length (mm) from one cross-section to the next, and the area of cross-section i.
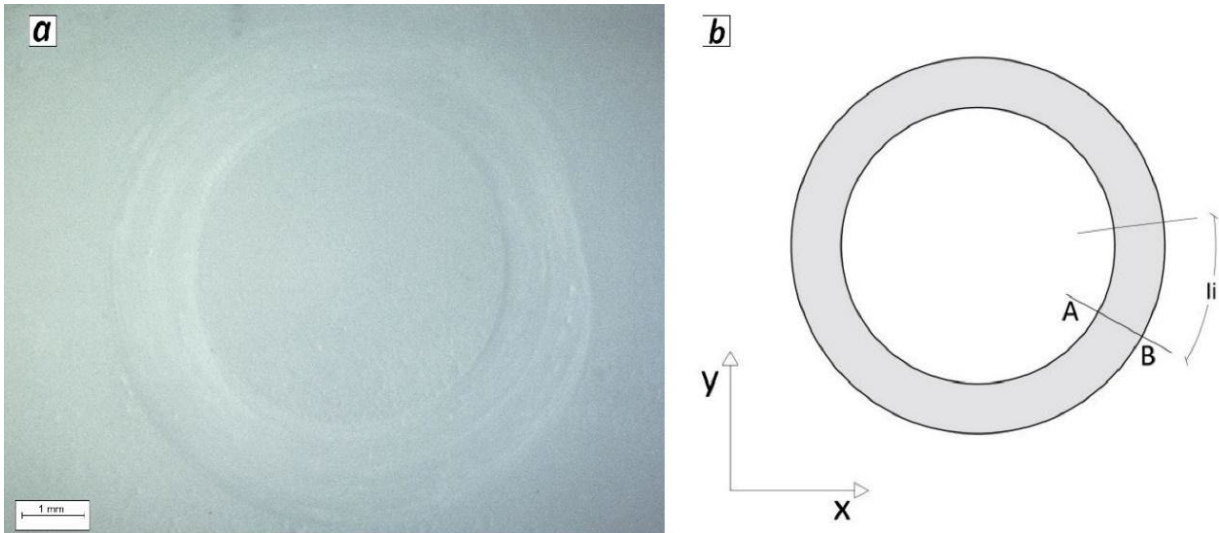
Figure 9. Micrograph of wear track (a) and wear track geometric model (b).

Since each wear track shows a circular arc shape (*Figure 10a*), the area of cross-section *i was* calculated according to a geometric model (*Figure 10b*) as the difference between the area of the circular sector $a_{circ\ sector_i}$ and the area of the triangle OAB, calculated by the equations (12), (13) and (14):

$$a_{circ\ sector_i} = \frac{1}{2}r_i^2\alpha_i \tag{12}$$

$$a_{AOB_i} = \frac{s_i\ (r_i - h_i)}{2} \tag{13}$$

$$h_i = r_i - \sqrt{r_i^2 - \frac{s_i^2}{4}}\ ;\ \alpha = 2\ arcsen\left(\frac{s_i}{2r_i}\right) \tag{14}$$

where r_i and α_i are the radius and the angle, respectively, of the circular sector, and s_i and h_i are the thickness and the depth, respectively, of wear track profile schematized in the geometric model used.
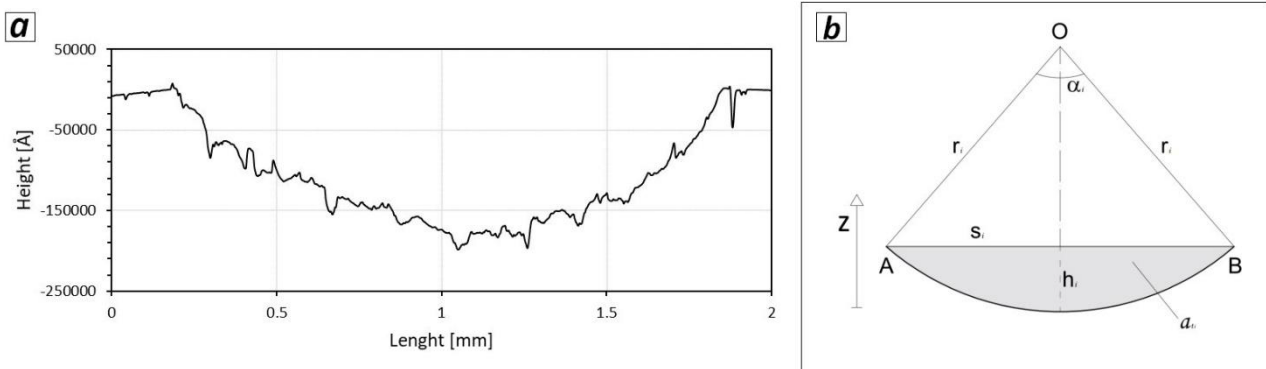

Figure 10. Profile of a wear track cross-section (a) and profile wear track geometric model (b).

SEM investigation on the worn surfaces allowed highlighting the mechanisms of the wear and friction. The wear tracks on the surface of the samples tested at 40 N in dry condition show a

13

succession of shiny and abraded areas; the worn areas with asportation are probably caused by the pin asperities or the presence of debris between the contact surfaces (*Figure 11a, Figure 11b*). The worn area appears smoother in lubrication (*Figure 11c, Figure 11d*) than in dry conditions.
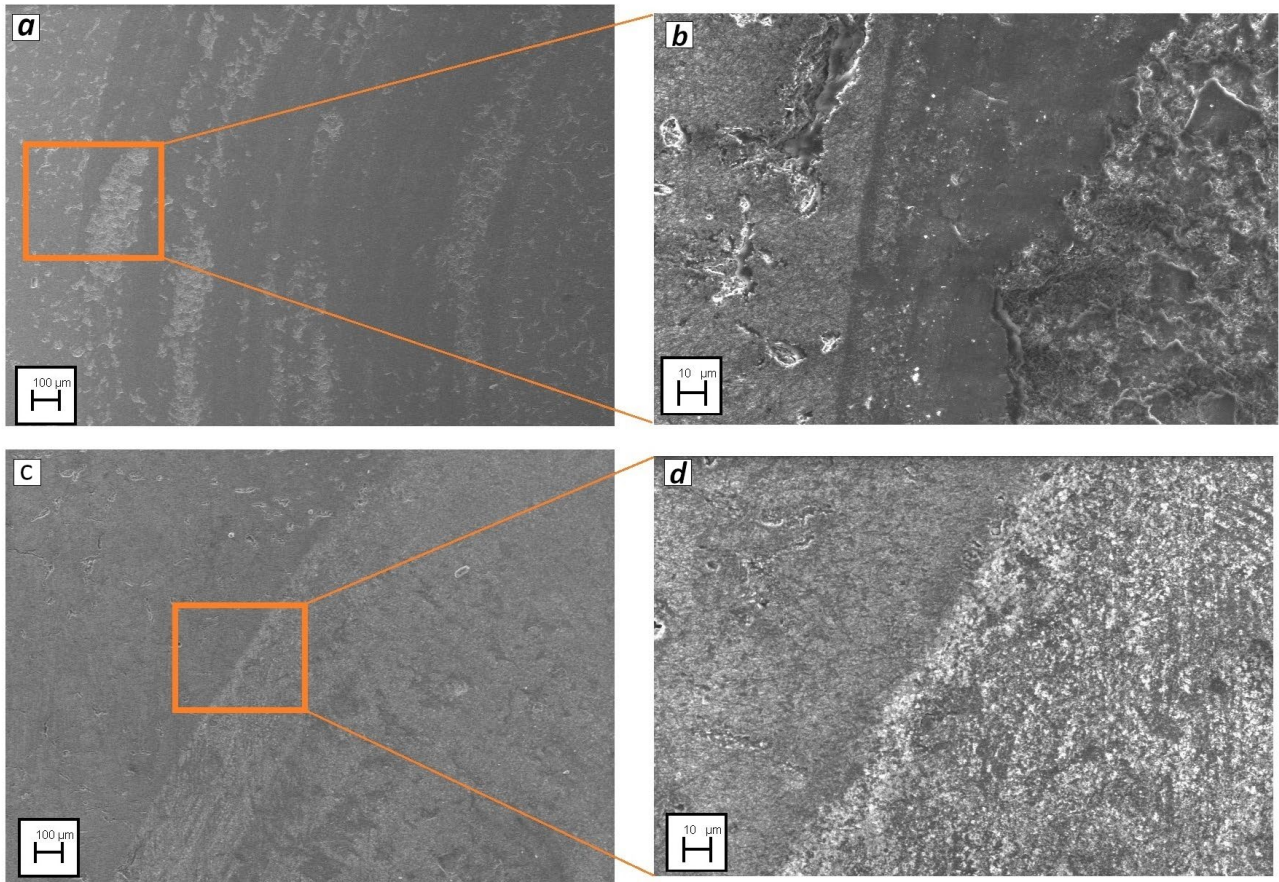
Figure 11. SEM micrographs of wear track at 40 N in DRY condition (a), DRY condition with higher magnification (b), BCS condition (c) and BCS condition with higher magnification (d).

The track measured by the profilometer shows an increase in width by increasing the contact pressure (*Table 5*). Track width increases to 33 and 77%, and 54 and 71% when contact pressure increases from 1500 to 2000 MPa, and from 1500 to 2500 MPa for non-aged and aged samples, respectively. A smaller increase in thickness was observed when using lubrication, with values up to 21 and 53%, and 32 and 44% from 1500 to 2000 MPa, and from 1500 to 2500 MPa, for non-aged and aged samples, respectively.

Mean contact pressure [MPa]; (Load [N])	Average wear track width [mm]			
	DRY	BCS	A-DRY	A-BCS
1500 (10)	0.34 ± 0.03	0.26 ± 0.02	0.31 ± 0.05	0.23 ± 0.05
2000 (20)	0.51 ± 0.02	0.33 ± 0.04	0.67 ± 0.07	0.34 ± 0.02
2500 (40)	1.51 ± 0.09	0.55 ± 0.05	1.06 ± 0.09	0.41 ± 0.03

Table 5. Average wear track width measured after tests at dry and lubricated conditions.

The average wear rate was low for all tests (*Table 6*) and at the initial mean contact pressure of 1500 MPa (10 N), the specific wear rate reached a maximum of about 10^{-6} mm^3/(N·m), and increased for all samples in dry conditions at 2000 and 2500 MPa.

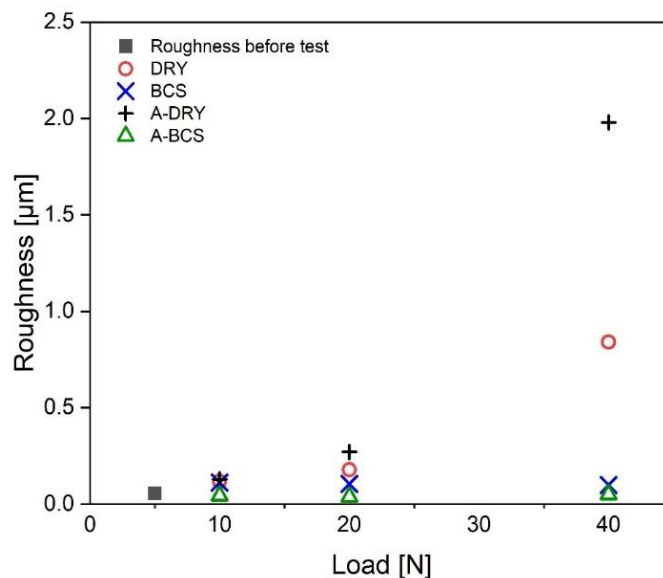| Mean contact pressure [MPa]; (Load [N])	k_w [mm^3/(N·m)]			
	DRY	BCS	A-DRY	A-BCS
1500 (10)	3.5E-06	1.9E-08	6.3E-06	2.4E-06
2000 (20)	1.3E-06	5.3E-08	2.1E-05	2.5E-06
2500 (40)	7.8E-05	3.6E-07	4.0E-05	2.6E-06

Table 6. Average wear rate [mm^3/(N·m)].

3.5 Roughness

The mean roughness (R_a) was calculated by equation (15) where the roughness of each profile (y_i) was calculated as the arithmetical mean of the absolute values of the deviations from the mean line of the roughness profile.

$$R_a = \frac{1}{n}\sum_{i=1}^{i=n}|y_i| \tag{15}$$

Ra of surface measured before each test shows a low value of 0.05 ± 0.02 µm. After the tests performed in dry conditions, the bottom of the track showed a slight increase of roughness at loads of 10 and 20 N and a high increase at 40 N (*Figure 12*). No significant variation of roughness was measured at lubricating conditions (*Table 7*).

Figure 12. Roughness in the wear track of ZTA materials during dry and lubricated conditions.

Mean contact pressure [MPa]; (Load [N])	Ra [μm]			
	DRY	BCS	A-DRY	A-BCS
1500 (10)	0.12 ± 0.08	0.11 ± 0.04	0.13 ± 0.04	0.04 ± 0.01
2000 (20)	0.18 ± 0.08	0.1 ± 0.1	0.27 ± 0.04	0.04 ± 0.01
2500 (40)	0.8 ± 0.2	0.1 ± 0.1	2.0 ± 0.2	0.05 ± 0.02

Table 7. Roughness in the wear track for ZTA materials during dry and lubricated conditions.

4   Discussion

A ZTA knee femoral prosthesis prototype made in Salentec srl by injection molding is shown in Figure 13. Tribological behavior of the prototypes was previously investigated in the knee wear simulator at the Rizzoli Orthopedic Institute in Bologna, with excellent results [41].

The complex shape of the prototype has been easily obtained from a mold with a single injection point. The forming phase from injection to demolding lasts one minute. This work aims to establish whether Ceramic Injection molding can be used in the intra-articular prosthesis sector.
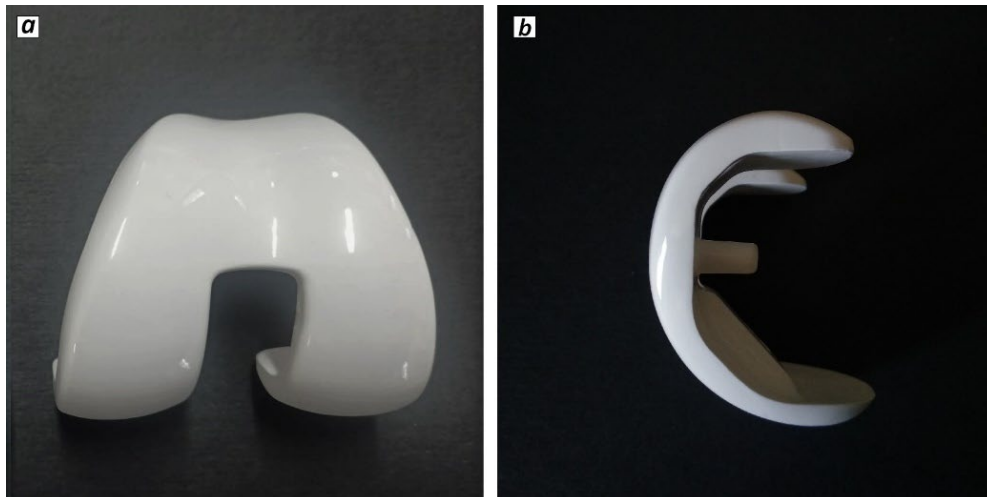

Figure 13. Salentec ZTA knee femoral prosthesis: front view (a) and side view (b).

A homogeneous distribution of the alumina and zirconia phases is revealed by SEM investigation of the ZTA material. Mean grain size and theoretical density are compliant with the requirements of the ISO 6474-2:2019 for the medical bone spacer, bone replacement, and components in orthopedic joint prostheses [31]. It is therefore confirmed that a homogeneous dispersion of zirconia grains in the alumina matrix with fine grain size, high densification degree and high hardness can be obtained by injection molding.

Mechanical properties which include a high value of Young's modulus (320 GPa), hardness (HV1 ~20 GPa), high fracture toughness (6.1 MPa·m$^{1/2}$) and high Weibull modulus (>17) confirm that CIM processed ZTA fulfils the structural requirements for ceramic material for medical applications [31]. These results havebeen compared to previous studies relative to ZTA prepare by CIM and cold

isostatic pressing (*Table 8*). Only the present study reached an apparent relative density (>99%) according request by the standards for orthopedic ceramic implants (hip or knee prosthesis) [31]. The good mechanical properties can be compare with Sequeira et al. cold isostatic pressing ZTA. Cold isostatic pressing is less accurate forming process and less efficient than CIM.

N.	Process	Composition [wt%]		Density [%]	Grain size [µm]		Hardness [GPa]	Flexural strength [MPa]	Toughness [MPa·m$^{1/2}$]	References
		Alumina	Zirconia		Alumina	Zirconia				
1	CIM (sint. temp: 1500°C/2 h)	85	15	~94 - 95	~1	~0.4	~22	~580	~5.2 (by micro-indentation)	Abou el Ezz et al. [42]
2	CIM (sint. temp: 1650°C/2 h)	80	20	~97	-	-	~20	~334	-	Chuankrerkkul et al. [43]
3	CIM (sint. temp: 1560°C/2 h)	80-90	10~20	~97.7	-	~0.39	~19.42	-	~5.2	H.S. Kim et al. [44]
4	CIM (sint. temp: 1700°C/2 h)	85	15	97-98	-	-	~17	~355	-	Chuankrerkkul et al. [47]
5	Cold isostatic pressing (sint. temp: 1400°C/3 h)	80	20	98.4	~0.46	~0.25	~18	~900	~5	Sequeira et al. [13]
6	CIM (sint. temp: 1475°C/75 min)	83	17	99.4	~1.15	~0.6	~20	~515	~6.1	ZTA OF CURRENT STUDY

Table 8. Physical and mechanical properties of ZTA ceramic of this research compared to other studies.

An important focus was on the performance of the ZTA *in vivo*, i.e., evaluating the stability of the zirconia tetragonal phase under an aqueous environment at body temperature. Tetragonal to monoclinic phase transformation can cause embrittlement of the arthroplasty components [45]. Deville et al. evaluated that 1 hour of autoclave treatment at 134°C has theoretically the same effect as 3 to 4 years *in vivo* at 37°C. In this way, several experimental tests on animals or patients can be avoided [27]. In this study selected samples were subjected to accelerated aging in an autoclave for 10 h before monoclinic content and mechanical properties evaluation.

Chevalier et al. claimed that the XRD method is not very accurate for quantifying monoclinic contents <5%, however the low monoclinic phase obtained by this method were similar to values recorded by Raman spectroscopy i.e 3.4 and 4.5% for non-aged and aged samples respectively [21], [46].

Flexural strength reduction due to hydrothermal aging, which should be less than 20% of the value before autoclaving [31], was not observed; the flexural strength evaluated for the samples before and after aging is approximately equal to 500 MPa and Young's modulus remain unaltered. According to published results [13], the 10 hours ageing treatment is not deleterious to the mechanical properties.

The failure mechanism has been carefully evaluated through SEM analyses of the fracture surfaces. The origin of fracture has been identified in correspondence of large pores located nearby the higher tensile stress. The fracture mirror typical of crystalline ceramics was visible in the SEM micrographs. Griffith's model allowed estimation of the fracture stress (σ_f) in the defect site [48] and to compare it to the flexural strength (σ_d) calculated at the same site. A good correspondence was found.

The results of tribological testing on the ceramic-on-ceramic, performed by in pin-on-disk tribometer showed a stable friction coefficient of 0.34, 0.21 and 0.11 for unaged samples at Hertzian pressures of 1500, 2000 and 2500 MPa, in dry conditions and slightly higher values for aged samples. For

lubricated test conditions, the mean friction coefficient (~ 0.08) did not show a significant change with varying load. This reduction of friction coefficient in comparison to the dry condition is consistent with previous studies. Marin et al. tested commercially available ZTA femoral head using a pin-on-ball wear tester in the ceramic-on-ceramic configuration under dry and under lubricating conditions at a maximum contact pressure of 1100 MPa, and obtained friction coefficient of 0.53, 0.49 and 0.27 in dry, water and squalene conditions respectively [23]. Shankar et al. tested zirconia ball against alumina disk using a ball-on-disk tribometer in dry and lubrication conditions that represent quite realistic wear behavior of femoral head sliding against a cup of arthroplasty implant: contact pressure of 1500 MPa, friction coefficients of 0.37 and 0.10 in dry and lubricated conditions respectively were recorded [49] and they are quite similar to values found in the present study at the same contact pressure.

Specific wear rate (k_w) was low for all materials: a value of 10^{-6} mm^3/(N·m) at the initial mean contact pressure of 1500 MPa was calculated but a significant increase was observed at dry conditions. This result is in agreement with tribological investigations of Kerkwijk et al. on different ceramics tested in a pin-on-disk tribometer at varying loads and dry conditions. They observed a specific wear rate below 10^{-6} mm^3/(N·m) for ZTA at the initial pressure up to 1600 MPa, and a friction coefficient equal to 0.45 evaluated at 1500 MPa [50]. SEM analysis of worn surfaces confirmed that lubrication conditions played a significant role in Ceramic-on-Ceramic coupling, minimizing friction and wear, desirable condition for artificial joint implants [35]. The micrographs of wear tracks showed an alternate of smoothed areas and abraded areas. The abrasion was probably due to the pin asperities or the presence of debris between the contact surfaces in dry conditions as described by Kerkwijk et al. [50]. The worn area appeared smoother in lubrication than in dry conditions.

The mean roughness (Ra) of the surface measured before each wear test showed a low value equal to 0.05 ± 0.02 μm, which is in accordance with the limits of roughness (0.1 μm) for ceramic femoral and tibial components of knee joint replacement [51]. A slight increase of roughness in the bottom of the wear track was measured after the tests performed in the dry condition for loads of 10 and 20 N and a higher increase at 40 N for all samples. Low friction coefficient between ZTA contact surfaces (0.08 - 0.13 and 0.05 - 0.07 in lubricated condition, 0.11 - 0.34 and 0.16 - 0.36 in dry condition for unaged and aged ZTA respectively) and low wear rate was measured by the tribological tests. These results show good mechanical and tribological properties were maintained even after the ageing of the material. No significant variation of roughness was measured in lubricating conditions. These results are compliant with the tribological investigation on state of art femoral heads [23].

5 Conclusion

Knee femoral prosthesis prototypes were developed in dense and homogeneous zirconia toughened alumina by ceramic injection molding. Microstructural, mechanical and tribological performances were investigated and the obtained properties were: toughness (6.1 MPa·m$^{1/2}$), hardness (20 GPa), Young's modulus (320 GPa), flexural strength (515 MPa), low and constant friction coefficient and negligible wear. Some pores were found on the fractured surface after flexural tests attributed to an imperfect filling of the mold during the injection phase of the CIM process. The origin of fracture was identified in these defects and the Griffith's model confirms the correlation between strength and defect/pore size revealed in the fractured surface of test bars. Further studies are currently ongoing on the process optimization.

To simulate in vivo ageing, an accelerated aging by autoclave was performed and the results indicate that microstructural, mechanical and tribological properties of the ZTA did not change after aging although a small increase in monoclinic zirconia was detected.

Aknowledgments

References:

[1]   J. A. Singh, S. Yu, L. Chen, and J. D. Cleveland, 'Rates of Total Joint Replacement in the United States: Future Projections to 2020–2040 Using the National Inpatient Sample', *J Rheumatol*, vol. 46, no. 9, pp. 1134–1140, Sep. 2019, doi: 10.3899/jrheum.170990.

[2]   S. Kurtz, K. Ong, E. Lau, F. Mowat, and M. Halpern, 'Projections of Primary and Revision Hip and Knee Arthroplasty in the United States from 2005 to 2030':, *The Journal of Bone & Joint Surgery*, vol. 89, no. 4, pp. 780–785, Apr. 2007, doi: 10.2106/JBJS.F.00222.

[3]   R. E. Guerrero-Ludueña *et al.*, 'Predicting the Burden of Revision Knee Arthroplasty: Simulation of a 20-Year Horizon', *Value in Health*, vol. 19, no. 5, pp. 680–687, Jul. 2016, doi: 10.1016/j.jval.2016.02.018.

[4]   McKee GK and Watson-Farrar J., 'Replacement of arthritic hips by the McKee-Farrar prosthesis', *J Bone Joint Surg Br.*, vol. 48, no. 2, pp. 245–259, 1966.

[5]   P. Triclot, 'Metal-on-metal: history, state of the art (2010)', *International Orthopaedics (SICOT)*, vol. 35, no. 2, pp. 201–206, Feb. 2011, doi: 10.1007/s00264-010-1180-8.

[6]   I. D. Learmonth, C. Young, and C. Rorabeck, 'The operation of the century: total hip replacement', *The Lancet*, vol. 370, no. 9597, pp. 1508–1519, Oct. 2007, doi: 10.1016/S0140-6736(07)60457-7.

[7]   T. Vu-Han, S. Hardt, R. Ascherl, C. Gwinner, and C. Perka, 'Recommendations for return to sports after total hip arthroplasty are becoming less restrictive as implants improve', *Arch Orthop Trauma Surg*, vol. 141, no. 3, pp. 497–507, Mar. 2021, doi: 10.1007/s00402-020-03691-1.

[8]   J. P. Kretzer *et al.*, 'Wear in total knee arthroplasty—just a question of polyethylene?: Metal ion release in total knee arthroplasty', *International Orthopaedics (SICOT)*, vol. 38, no. 2, pp. 335–340, Feb. 2014, doi: 10.1007/s00264-013-2162-4.

[9]   Z. M. Jin, J. Zheng, W. Li, and Z. R. Zhou, 'Tribology of medical devices', *Biosurface and Biotribology*, vol. 2, no. 4, pp. 173–192, Dec. 2016, doi: 10.1016/j.bsbt.2016.12.001.

[10]   P. Boutin, 'Total arthroplasty of the hip by fritted alumina prosthesis. Experimental study and 1st clinical applications', *Orthopaedics & Traumatology: Surgery & Research*, vol. 100, no. 1, pp. 15–21, Feb. 2014, doi: 10.1016/j.otsr.2013.12.004.

[11]   L. Sedel, 'Evolution of Alumina-on-Alumina Implants: A Review', *Clinical Orthopaedics and Related Research*, vol. 379, pp. 48–54, Oct. 2000, doi: 10.1097/00003086-200010000-00008.

[12]   A. A. Porporati, C. Piconi, M. Mettang, U. Deisinger, C. Reinhardt, and R. Pitto, 'Ceramics for artificial joints: The relevance of material biocompatibility', in *Bioceramics*, Elsevier, 2021, pp. 263–295. doi: 10.1016/B978-0-08-102999-2.00012-0.

[13] S. Sequeira, M. H. Fernandes, N. Neves, and M. M. Almeida, 'Development and characterization of zirconia–alumina composites for orthopedic implants', *Ceramics International*, vol. 43, no. 1, pp. 693–703, Jan. 2017, doi: 10.1016/j.ceramint.2016.09.216.

[14] S. Xiang, Y. Zhao, Z. Li, B. Feng, and X. Weng, 'Clinical outcomes of ceramic femoral prosthesis in total knee arthroplasty: a systematic review', *J Orthop Surg Res*, vol. 14, no. 1, p. 57, Dec. 2019, doi: 10.1186/s13018-019-1090-4.

[15] I. C. Clarke *et al.*, 'Ultra-low wear rates for rigid-on-rigid bearings in total hip replacements', *Proc Inst Mech Eng H*, vol. 214, no. 4, pp. 331–347, Apr. 2000, doi: 10.1243/0954411001535381.

[16] M. Kuntz and R. Krüger, 'The effect of microstructure and chromia content on the properties of zirconia toughened alumina', *Ceramics International*, vol. 44, no. 2, pp. 2011–2020, Feb. 2018, doi: 10.1016/j.ceramint.2017.10.146.

[17] A. H. De Aza, J. Chevalier, G. Fantozzi, M. Schehl, and R. Torrecillas, 'Crack growth resistance of alumina, zirconia and zirconia toughened alumina ceramics for joint prostheses', *Biomaterials*, vol. 23, no. 3, pp. 937–945, Feb. 2002, doi: 10.1016/S0142-9612(01)00206-X.

[18] J. R. T. Jeffers and W. L. Walter, 'Ceramic-on-ceramic bearings in hip arthroplasty: State of the art and the future', *The Journal of Bone and Joint Surgery. British volume*, vol. 94-B, no. 6, pp. 735–745, Jun. 2012, doi: 10.1302/0301-620X.94B6.28801.

[19] J. L. Masonis, R. B. Bourne, M. D. Ries, R. W. McCalden, A. Salehi, and D. C. Kelman, 'Zirconia femoral head fractures', *The Journal of Arthroplasty*, vol. 19, no. 7, pp. 898–905, Oct. 2004, doi: 10.1016/j.arth.2004.02.045.

[20] E. M. Santos, S. Vohra, S. A. Catledge, M. D. McClenny, J. Lemons, and K. D. Moore, 'Examination of surface and material properties of explanted zirconia femoral heads', *The Journal of Arthroplasty*, vol. 19, no. 7, pp. 30–34, Oct. 2004, doi: 10.1016/j.arth.2004.06.017.

[21] J. Chevalier, 'What future for zirconia as a biomaterial?', *Biomaterials*, vol. 27, no. 4, pp. 535–543, Feb. 2006, doi: 10.1016/j.biomaterials.2005.07.034.

[22] J. Rieu and P. Goeuriot, 'Ceramic composites for biomedical applications', *Clin. Mater.*, vol. 12, pp. 211–217, 1993.

[23] E. Marin, A. Rondinella, W. Zhu, B. J. McEntire, B. S. Bal, and G. Pezzotti, 'Wear and surface degradation of commercial ZTA femoral heads under boundary lubrication conditions', *Journal of the Mechanical Behavior of Biomedical Materials*, vol. 65, pp. 616–626, Jan. 2017, doi: 10.1016/j.jmbbm.2016.09.038.

[24] S. M. Kurtz, S. Kocagöz, C. Arnholt, R. Huet, M. Ueno, and W. L. Walter, 'Advances in zirconia toughened alumina biomaterials for total joint replacement', *Journal of the Mechanical Behavior of Biomedical Materials*, vol. 31, pp. 107–116, Mar. 2014, doi: 10.1016/j.jmbbm.2013.03.022.

[25] C. Y. Hu and T.-R. Yoon, 'Recent updates for biomaterials used in total hip arthroplasty', *Biomater Res*, vol. 22, no. 1, p. 33, Dec. 2018, doi: 10.1186/s40824-018-0144-8.

[26] V. Naglieri, P. Palmero, L. Montanaro, and J. Chevalier, 'Elaboration of Alumina-Zirconia Composites: Role of the Zirconia Content on the Microstructure and Mechanical Properties', *Materials*, vol. 6, no. 5, pp. 2090–2102, May 2013, doi: 10.3390/ma6052090.

[27] S. Deville, L. Gremillard, J. Chevalier, and G. Fantozzi, 'A critical comparison of methods for the determination of the aging sensitivity in biomedical grade yttria-stabilized zirconia', *J. Biomed. Mater. Res.*, vol. 72B, no. 2, pp. 239–245, Feb. 2005, doi: 10.1002/jbm.b.30123.

[28] E. Meier, K. Gelse, K. Trieb, M. Pachowsky, F. F. Hennig, and A. Mauerer, 'First clinical study of a novel complete metal-free ceramic total knee replacement system', *J Orthop Surg Res*, vol. 11, no. 1, p. 21, Dec. 2016, doi: 10.1186/s13018-016-0352-7.

[29] M. F. Saccomanno *et al.*, 'Allergy in total knee replacement surgery: Is it a real problem?', *WJO*, vol. 10, no. 2, pp. 63–70, Feb. 2019, doi: 10.5312/wjo.v10.i2.63.

[30] D. Glaser, R. D. Komistek, H. E. Cates, and M. R. Mahfouz, 'Clicking and Squeaking: In Vivo Correlation of Sound and Separation for Different Bearing Surfaces', *Journal of Bone and Joint Surgery*, vol. 90, no. Supplement_4, pp. 112–120, Nov. 2008, doi: 10.2106/JBJS.H.00627.

[31] 'ISO 6474-2:2019, Implant for surgery - Ceramic materials- Part 2: Composite materials based on a high-purity alumina matrix with zirconia reinforcement', ISO 6474-2. Implant for surgery - Ceramic materials - Part 2: Composite materials based on a high-purity alumina matrix with zirconia reinforcement', 2019.

[32] M. A. Elezz, F. Kern, and R. Gadow, 'Manufacturing of ZTA composites for biomedical applications', in *2012 International Conference on Engineering and Technology (ICET)*, Cairo, Egypt, Oct. 2012, pp. 1–5. doi: 10.1109/ICEngTechnol.2012.6396123.

[33] L. B. McCusker, R. B. Von Dreele, D. E. Cox, D. Louër, and P. Scardi, 'Rietveld refinement guidelines', *J Appl Crystallogr*, vol. 32, no. 1, pp. 36–50, Feb. 1999, doi: 10.1107/S0021889898009856.

[34] 'UNI EN ISO 23146:2016, Fine ceramics (advanced ceramics, advanced technical ceramics) - Test methods for fracture toughness of monolithic ceramics - Single-edge V-notch beam (SEVNB) method', 2016.

[35] S. Ghosh, D. Choudhury, T. Roy, A. Moradi, H. H. Masjuki, and B. Pingguan-Murphy, 'Tribological performance of the biological components of synovial fluid in artificial joint implants', *Science and Technology of Advanced Materials*, vol. 16, no. 4, p. 045002, Jul. 2015, doi: 10.1088/1468-6996/16/4/045002.

[36] N. R. Tedesco, E. M. J. A. Pallone, and R. Tomasi, 'Effects of the Pin-on-Disc Parameters on the Wear of Alumina', Oct. 2010, pp. 39–44. doi: 10.4028/www.scientific.net/AST.65.39.

[37] H. Toraya, M. Yoshimura, and S. Sōmiya, '"Calibration Curve for Quantitative Analysis of the Monoclinic-Tetragonal ZrO2 System of X-Ray Diffraction", Communications of the American Ceramic Society, p. C-119-C–121', 1984.

[38] A. C. O. Lopes *et al.*, 'Nanomechanical and microstructural characterization of a zirconia-toughened alumina composite after aging', *Ceramics International*, vol. 45, no. 7, pp. 8840–8846, May 2019, doi: 10.1016/j.ceramint.2019.01.211.

[39] J. A. Williams and R. S. Dwyer-Joyce, '"Contact Between Solid Surfaces", p. 42', 2001.

[40] B. Kerkwijk, L. Winnubst, E. J. Mulder, and H. Verweij, 'Processing of Homogeneous Zirconia-Toughened Alumina Ceramics with High Dry-Sliding Wear Resistance', *Journal of the American Ceramic Society*, vol. 82 (8), pp. 2087–2093, 1999.

[41] S. Affatato, P. Erani, M. Fersini, V. Contaldi, A. R. Terrizzi, and A. Licciulli, 'Preliminary In Vitro Wear Assessment of Ceramic Cemented Femoral Components Coupled with Polyethylene Menisci', *Materials*, vol. 14, no. 9, p. 2112, Apr. 2021, doi: 10.3390/ma14092112.

[42] M. Abou el Ezz, 'Ageing Behavior of Injection-Molded ZTA Ceramics as a Function of Stabilizer Content', *J. Ceram. Sci. Tech.*, no. 04, 2011, doi: 10.4416/JCST2011-00025.

[43] N. Chuankrerkkul, R. Charoenkijmongkol, P. Somboonthanasarn, C. Auechalitanukul, and R. C. McCuiston, 'Microstructure and Properties of Zirconia Toughened Alumina Fabricated by Powder Injection Moulding', *KEM*, vol. 659, pp. 116–120, Aug. 2015, doi: 10.4028/www.scientific.net/KEM.659.116.

[44] H. S. Kim, M. Y. Seo, and I. J. Kim, 'Densification and Thermo-Mechanical Properties of Al2O3-ZrO2 (Y2O3) Composites', *Journal of the Korean Ceramic Society*, vol. 43, no. 9, pp. 515–518, 2006, doi: https://doi.org/10.4191/KCERS.2006.43.9.515.

[45] M. Boffelli *et al.*, 'Chemically driven tetragonal-to-monoclinic polymorphic transformation in retrieved ZTA femoral heads from dual mobility hip implants', *Journal of the Mechanical Behavior of Biomedical Materials*, vol. 56, pp. 195–204, Mar. 2016, doi: 10.1016/j.jmbbm.2015.11.032.

[46] J. Chevalier, L. Gremillard, and S. Deville, 'Low-Temperature Degradation of Zirconia and Implications for Biomedical Implants', *Annu. Rev. Mater. Res.*, vol. 37, no. 1, pp. 1–32, Aug. 2007, doi: 10.1146/annurev.matsci.37.052506.084250.

[47] 'Chuankrerkkul e Dateraksa - Physical and Mechanical Properties of Zirconia Tou.pdf'.

[48] G. D. Quinn, 'NIST Recommended Practice Guide: Fractography of Ceramics and Glasses', National Institute of Standards and Technology, Sep. 2020. doi: 10.6028/NIST.SP.960-16e3.

[49] S. Shankar, R. Nithyaprakash, P. Sugunesh, M. Uddin, and A. Pramanik, 'Contact Stress and Wear Analysis of Zirconia Against Alumina for Normal and Physically Demanding Loads in Hip Prosthesis', *J Bionic Eng*, vol. 17, no. 5, pp. 1045–1058, Sep. 2020, doi: 10.1007/s42235-020-0078-4.

[50] B. Kerkwijk, A. J. A. Winnubst, H. Verweij, E. J. Mulder, H. S. C. Metselaar, and D. J. Schipper, 'Tribological properties of nanoscale alumina–zirconia composites', *Wear*, vol. 225–229, pp. 1293–1302, Apr. 1999, doi: 10.1016/S0043-1648(98)00403-7.

[51] 'ISO 7207-2:2011/Amd 1:2016, Implants for surgery - Components for partial and total knee joint prostheses - Part 2: Articulating surfaces made of metal, ceramic and plastics materials - Amendment 1', 2016.